D-*threo*-1-Phenyl-2-decanoylamino-3-morpholino-1-propanol Alters Cellular Cholesterol Homeostasis by Modulating the Endosome Lipid Domains†

Asami Makino,‡ Kumiko Ishii,‡ Motohide Murate,‡ Tomohiro Hayakawa,‡ Yusuke Suzuki,‡ Minoru Suzuki,‡ Kazuki Ito,‡ Tetsuro Fujisawa,‡ Hirotami Matsuo,§ Reiko Ishitsuka,‡ and Toshihide Kobayashi*,‡,||

RIKEN Wako-shi, Saitama 351-0198, Japan, School of Pharmacy, Shujitsu University, Okayama 703-8516, Japan, and INSERM U585, INSA-Lyon, 69621 Villeurbanne, France

Received October 15, 2005; Revised Manuscript Received February 2, 2006

ABSTRACT: D-*threo*-1-Phenyl-2-decanoylamino-3-morpholino-1-propanol (D-PDMP) is a frequently used inhibitor of glycosphingolipid biosynthesis. However, some interesting characteristics of D-PDMP cannot be explained by the inhibition of glycolipid synthesis alone. In the present study, we showed that D-PDMP inhibits the activation of lysosomal acid lipase by late endosome/lysosome specific lipid, bis-(monoacylglycero)phosphate (also called as lysobisphosphatidic acid), through alteration of membrane structure of the lipid. When added to cultured fibroblasts, D-PDMP inhibits the degradation of low-density lipoprotein (LDL) and thus accumulates both cholesterol ester and free cholesterol in late endosomes/lysosomes. This accumulation results in the inhibition of LDL-derived cholesterol esterification and the decrease of cell surface cholesterol. We showed that D-PDMP alters cellular cholesterol homeostasis in a glycosphingolipid-independent manner using L-PDMP, a stereoisomer of D-PDMP, which does not inhibit glycosphingolipid synthesis, and mutant melanoma cell which is defective in glycolipid synthesis. Altering cholesterol homeostasis by D-PDMP explains the unique characteristics of sensitizing multidrug resistant cells by this drug.

D-*threo*-1-Phenyl-2-decanoylamino-3-morpholino-1-propanol (D-PDMP)[1] is a well recognized inhibitor of UDP-glucose: ceramide glucosyltransferase (EC 2.4.1.80; GlcCer synthase (GCS)) (*1*, *2*). However, several interesting characteristics of D-PDMP, such as the chemosensitization of multidrug resistant cancer cells (*3*−*9*) and the enhancement of cholesterol efflux (*10*), cannot be explained by the inhibition of GCS alone (*11*). Previously it was shown that PDMP accumulates cholesterol intracellularly (*12*). It has been reported that D-PDMP alteration of cellular cholesterol content depends on the cell type (*13*, *14*). This effect of D-PDMP has been explained as a result of trapping cholesterol within glycosphingolipid (GSL)-laden compartments due to physical association of cholesterol with GSLs (*13*). In the present study, we demonstrate that D-PDMP accumulates in late endosomes/lysosomes. A characteristic feature of this organelle is its multivesicular structure (*15*, *16*). The internal membranes of late endosomes are highly enriched with a unique acidic phospholipid, lysobisphosphatidic acid (LBPA, also called bis(monoacylglycero)-phosphate (BMP); according to the suggestion of Kolter and Sandhoff (*17*) we use the abbreviation BMP throughout the text) (*18*−*20*). Recently a BMP rich membrane domain has been shown to be involved in both membrane traffic from late endosomes and the degradation of sphingolipids in the organelle (*17*, *21*−*22*). BMP is also involved in the formation of multivesicular membranes, suggesting that the characteristic membrane structure is indeed a prerequisite for the proper function of this membrane domain (*23*). The addition of D-PDMP modulated the structure of the BMP membrane in a pH-dependent manner and inhibited the BMP-enhanced acid lipase activity in vitro. In cultured cells, D-PDMP inhibited the degradation of LDL. As a result, intracellular cholesterol accumulated and the cell surface cholesterol decreased. This decrease altered P-glycoprotein activity leading to enhanced uptake of the anticancer reagent.

MATERIALS AND METHODS

Cells and Reagents. Cultured human skin fibroblasts were established as described (*21*). Cells were maintained in F10 medium supplemented with 10% fetal calf serum (FCS), 100 units/mL penicillin, and 100 μg/mL streptomycin. A glycosphingolipid-deficient mutant cell line of mouse melanoma, GM95 (*24*), was a generous gift of Dr. Y. Hirabayashi (Brain Science Institute, RIKEN, Japan). The cells were cultured

† This work was supported by grants from the Ministry of Education, Science, Sports and Culture of Japan (16044247 and 17390025 to T.K., 16790073 to A.M., 17659058 to M.M., and 16770083 to R.I.), grants from RIKEN Frontier Research System, Chemical Biology Research Project of RIKEN, and a grant from Ono Medical Research Foundation (to T.K.), and a Grant from Kato Memorial Bioscience Foundation (to H.M.).

* To whom correspondence should be addressed. Mailing address: RIKEN, 2-1, Hirosawa, Wako-shi, Saitama 351-0198, Japan. Tel: +81-48-467-9612. Fax: +81-48-467-8693. E-mail:kobayasi@riken.jp.

‡ RIKEN.

§ Shujitsu University.

|| INSA (Institut National des Sciences Appliquees).

[1] Abbreviations: D-PDMP, D-*threo*-1-phenyl-2-decanoylamino-3-morpholino-1-propanol; BMP, bis(monoacylglycero)phosphate; C6-NBD-Cer, 6-((*N*-(7-nitrobenz-2-oxa-1,3-diazol-4-yl)amino)hexanoyl)-sphingosine; GCS, UDP-glucose: ceramide glucosyltransferase, GlcCer synthase; GSL, glycosphingolipid; L-PDMP, L-*threo*-1-phenyl-2-decanoylamino-3-morpholino-1-propanol; LBPA, lysobisphosphatidic acid; LDL, low-density lipoprotein; MDR, multidrug resistance; *N*B-DNJ, *N*-butyl-deoxynojirimycin.

10.1021/bi052104y CCC: $33.50
Published on Web 03/18/2006

in DMEM supplemented with 10% FCS, 100 units/mL penicillin, and 100 μg/mL streptomycin. Baby hamster kidney cells were grown as described (*18*). Murine neuroblastoma, Neuro-2a, was provided by Dr. H. Higashi (Brain Science Institute, RIKEN, Japan). The cells were grown in DMEM supplemented with 5% FCS, 100 units/mL penicillin, and 100 μg/mL streptomycin. D-*threo*-1-Phenyl-2-decanoylamino-3-morpholino-1-propanol (D-PDMP) and L-*threo*-1-phenyl-2-decanoylamino-3-morpholino-1-propanol (L-PDMP) were from Matreya Inc. (Pleasant Gap, PA). *N*-Butyldeoxynojirimycin (*N*B-DNJ), filipin, 25-hydroxycholesterol, and human lipoprotein-deficient serum were obtained from Sigma (St. Louis, MO). U18666A was from BioMol (Plymouth Meeting, PA). 6-((*N*-(7-Nitrobenz-2-oxa-1,3- diazol-4-yl)amino)hexanoyl)sphingosine (C6-NBD-Cer), cholesteryl 4,4-difluoro-5,7-dimethyl-4-bora-3a,4a-diaza-*s*-indacene-3-dodecanoate (cholesteryl BODIPY FL C12), nile red, and paclitaxel BODIPY FL conjugate (BODIPY FL paclitaxel) were from Molecular Probes (Eugene, OR). Anti-CD63 antibody was purchased from Cymbus Biotechnology Ltd. (Chandlers Ford, U.K.). 4-methylumbelliferyl oleate was from Fluka (St. Louis, MO). Anti-bis(monoacylglycero)-phosphate (BMP) antibody (anti-lysobisphosphatidic acid (LBPA) antibody) was prepared as described (*18*). [^{14}C]Oleic acid (50.0 mCi/mmol) and [cholesteryl-4-^{14}C] oleate (55 mCi/mmol) were from American Radiolabeled Chemicals Inc. (St. Louis, MO). Streptolysin O was obtained from Dr. Sucharit Bhakdi (Johannes Gutenberg Universitat, Mainz, Germany). LDL was prepared by ultracentrifugation. [Cholesteryl-4-^{14}C] oleate-containing LDL (16 μCi/mg protein) and cholesteryl BODIPY FL C12-containing LDL (350 μM fluorophore/mg protein) were prepared as described (*25*).

Cell Staining. All manipulations were done at room temperature. Cells grown on coverslips were washed with phosphate buffered saline (PBS) and then were fixed for 20 min with 3% paraformaldehyde in PBS. The cells were washed with PBS and quenched with 50 mM NH_4Cl for 15 min. After washing with PBS, cells were permeabilized by treating with 50 μg/mL digitonin for 5 min. The specimens were blocked with 0.2% gelatin in PBS for 30 min. After 30 min treatment with the first antibody, cells were washed and labeled with the fluorescent second antibody. When cholesterol was stained, 50 μg/mL filipin was added in both primary and secondary antibody solutions. Nile red (100 ng/mL) was added in the second antibody solution. The stained cells were washed and mounted in Mowiol and examined under a Zeiss LSM 510 confocal microscope equipped with C-Apochromat 63XW Korr (1.2 n.a.) objective. When cells were labeled with nile red, the dye was included in Mowiol.

Measurement of Glycolipid Synthesis. Human skin fibroblasts were grown on 60 mm plastic culture dishes for 3 days in the presence of various concentration of D-PDMP, L-PDMP, or *N*B-DNJ. Cells were then washed with serum free medium. The culture medium was then changed to the serum free medium containing 5 μM C6-NBD-Cer prepared by adding a 5 mM ethanol solution of the fluorescent lipid to F10 medium. After 1 h incubation, cells were harvested using a rubber policeman and lipids extracted (*26*, *27*) after protein measurement. Extracted lipids were applied to an HPTLC plate (Merck) and developed in $CHCl_3/CH_3OH/H_2O$ (65:25:4). Fluorescent lipids were quantified using FLA3000 (Fuji film, Tokyo, Japan), and the fluorescence intensity was normalized against protein concentration.

Electron Microscopy. Human skin fibroblasts were grown on fibronectin-coated Aclar plastic sheets (Nisshin EM, Tokyo, Japan) for 2 days in the presence and absence of 10 μM D-PDMP. Cells were then fixed for 30 min at room temperature with 4% paraformaldehyde and 2.5% glutaraldehyde in PBS, post-fixed with 1% osmium tetraoxide and 0.1 M imidazole, then stained with 0.2% tannic acid for 30 min. The samples were then dehydrated in the graded series of acetone, embedded in Araldite resin, and sectioned with ultramicrotome (Leica EM UC6, Vienna, Austria). Thin sections were stained with uranyl acetate and lead stain solution (Sigma-Aldrich Japan, Tokyo, Japan). For immunoelectron microscopy, D-PDMP-treated cells were grown on culture dishes, fixed with 4% paraformaldehyde and 0.05% glutaraldehyde in PBS. The cells were scraped off the dishes, pelleted, and embedded in low melting temperature agarose. Cell pellets were infused with 20% polyvinylpyrrolidone and 1.84 M sucrose and frozen in liquid propane cooled in liquid nitrogen. Ultrathin sections were cut with an ultracryomicrotome (EM UC6 and FC6, Leica, Austria), picked up in 1:1 (2.3 M sucrose):(2% methylcellulose). Labeling of BMP was performed with mouse monoclonal anti-BMP antibody and 10 nm colloidal gold conjugated-anti-mouse IgG antibody (Amersham Biosciences, Buckinghamshire, U.K.). After labeling, the sections were stained and embedded in 1.8% methylcellulose and 0.3% uranyl acetate. Both sections for conventional and immunoelectron microscopy were observed under a transmission electron microscope (JEOL 1200EX II, Tokyo, Japan). Electron micrographs recorded on imaging plates were scanned and digitized by an FDL 5000 imaging system (Fuji Photo Film, Tokyo, Japan).

Subcellular Fractionation and Lipid Analysis. Late endosomal fractions were prepared as described (*18*, *20*, *28*). Briefly, cells were homogenized, and then a post-nuclear supernatant was prepared. The post-nuclear supernatant was adjusted to 40.6% sucrose, 3 mM imidazole, pH 7.4, loaded at the bottom of an 50 Ultra clear tube (Beckman), and overlaid sequentially with 35% and 25% sucrose solutions in 3 mM imidazole, pH 7.4, and then homogenization buffer (HB; 250 mM sucrose, 3 mM imidazole, pH 7.4). The gradient was centrifuged for 60 min at 35 000 rpm using a Beckman MLS50 rotor. The late endosome fraction was collected at the 25% sucrose/HB interface. Lipids of the late endosome fraction were extracted and then separated by two-dimensional chromatography (*18*, *20*). The first direction was run with chloroform, methanol, and 32% ammonia (65:35:5 v/v) and the second direction with chloroform/acetone/methanol/acetic acid/water (10:4:2:2:1 v/v). Lipids were visualized by spraying primuline followed by UV detection.

Matrix-Assisted Laser Desorption/Ionization Time-of-Flight Mass Spectrometry. Matrix-assisted laser desorption/ionization time-of-flight mass spectrometry (MALDI-TOF MS) analysis was performed using an AXIMA-CFR (Shimadzu Corp., Kyoto, Japan) equipped with a 337 nm nitrogen laser. A saturated solution of 2,5-dihydroxybenzoic acid (DHB; Wako Pure Chemical Industries, Osaka, Japan) in water was used as the matrix, and the extracted and dried D-PDMP spot was dissolved in 6 μL of HPLC grade chloroform (Wako Pure Chemical Industries). The matrix

and D-PDMP solutions were mixed in equal proportions, and 4 μL aliquots of the resulting mixture were placed on a target plate for crystallization. Crystallization was accelerated by a gentle stream of cold air. Then, the target plate carrying cocrystals of matrix and analytes was introduced into the mass spectrometer. Mass spectra were calibrated externally with peaks from peptide calibration standard bradykinin fragments 1−7 (Sigma-Aldrich Japan) (*m*/*z* 757.40) and DHB (*m*/*z* 154.12).

Small-Angle X-ray Scattering (SAXS) Measurements. 2,2′-Dioleoyl-*sn* 1,1′-BMP was chemically synthesized as described previously (*29*). For X-ray measurements, dried films of 100 nmol of BMP were hydrated and vortexed with 100 μL buffer solutions that contained various drugs with 1 or 2.5 mM concentration, pelleted, and brought into a sample cell which had a path length of 1.5 mm and a pair of thin quartz windows (30 μm). The final concentration of BMP was approximately 2.5 mM. SAXS measurements were carried out at RIKEN Structural Biology Beamline I (BL-45XU) (*30*) at SPring-8, 8 GeV synchrotron radiation source, Hyogo, Japan. The X-ray wavelength used was 0.9 Å, and the beam size at the sample position was 0.4 × 0.7 mm^2. The distance of sample to detector was 851 mm. The sample temperature was controlled to 37.00 ± 0.01 °C with a high precision thermoelectric device. Buffer profiles were also taken for background subtraction purposes. The SAXS patterns were recorded with 30 s exposure by a beryllium-windowed X-ray image intensifier which was coupled with a cooled CCD camera (1000 × 1018 pixels) (*31*). The recorded images were applied to the required corrections (*32*). The two-dimensional powder diffraction patterns after the image distortion correction were circularly averaged and reduced to one-dimensional profiles using FIT2D version 12.012 (http://www.esrf.fr/computing/scientific/FIT2D/), a 2-D data reduction and analysis program. The reciprocal spacing (*s*) and scattering vectors (*q*),

$$s = 1/d = (2/\lambda)\sin\theta$$

$$q = 2\pi s = (4\pi/\lambda)\sin\theta$$

where *d* is the lattice spacing, 2θ is the scattering angle, and λ is the wavelength of X-ray, were calibrated with silver behenate by the long-period spacing of 5.838 nm (*33*).

Dynamic Light Scattering. The average hydrodynamic diameter of D-PDMP dispersions was measured at pH 4.6, 7.4, and 8.5 by a Malvern Zetasizer Nano ZS (ZEN3600), a DLS apparatus (Malvern Instruments Ltd., Worcester, England), using disposable square cells. Solution samples (0.5 mM) were subjected to scattering by monochromatic light (4.0 mW He−Ne laser, wavelength of 633 nm), and the scattering light intensity was measured at a scattering angle of 173°. All measurements were carried out at 37 °C. The particle sizes and polydispersities were calculated from the autocorrelation function of light scattering intensity with the Dispersion Technology Software package (Malvern Instruments Ltd., Worcester, England).

Measurement of Acid Lipase Activity. The acid lipase activity of the homogenate from human skin fibroblasts was measured as described using 4-methylumbelliferyl oleate as a substrate (*34*). Cell homogenate was prepared by sonication in 0.2 M citrate buffer, pH 4.6. BMP dispersions (100 μM) containing various amounts of D-PDMP were added to 24 μg/mL protein. The reaction was started by the addition of substrate (final concentration 100 nM), and the increase of fluorescence intensity at 449 nm (excitation at 327 nm) was monitored.

Uptake of Reconstituted LDL. Human skin fibroblasts were grown in F10 medium supplemented with 10% FCS, 100 units/mL penicillin, and 100 μg/mL streptomycin (medium A) in the presence and the absence of 10 μM D-PDMP. After 24 h of incubation, the medium was replaced with medium B (medium A in which 10% FCS is replaced with 5% human lipoprotein-deficient serum) with 10 μg/mL cholesteryl BODIPY FL C12-containing LDL in the presence and absence of 10 μM D-PDMP. After 5 h of incubation, a fluorescence image was acquired under a Zeiss LSM 510 confocal microscope quipped with a C-Apochromat 63XW Korr (1.2 n.a.) objective.

Hydrolysis of Cholesteryl-[4-^{14}C] Oleate-Containing LDL. Hydrolysis of LDL was measured using the following protocol (format 1): On day 0, monolayer stock flasks of human skin fibroblasts were trypsinized and seeded into a 3.5 cm dish in 1 mL of medium A. On day 1, monolayers were washed and the medium was changed to 1 mL of medium B. On day 3, cells were washed and the medium was replaced with 1 mL of medium C (medium B containing 20 μM mevinolin and 0.25 mM mevalonate) with and without inhibitors. On day 4, the medium was replaced with medium C with and without inhibitors in the presence of 10 μg/mL cholesteryl-[4-^{14}C] oleate-containing LDL (0.2 μCi/mL). After 2 h of incubation, the medium was replaced with fresh medium C with and without inhibitors. At appropriate intervals, lipids were extracted and the degradation of cholesteryl-[4-^{14}C] oleate to [4-^{14}C] cholesterol was quantified after separation of radioactive lipids on HPTLC, using hexane/diethyl ether/glacial acetic acid (80:20:2) as a solvent.

Measurement of Cellular Cholesterol and Cholesterol Ester Content. Human skin fibroblasts were grown on 60 mm plastic culture dishes for 3 days in the presence and absence of inhibitors. Cells were harvested using a rubber policeman, and protein was measured followed by lipid extraction (*35*). Extracted lipids were applied to an HPTLC plate (Merck) and developed in hexane/diethyl ether/glacial acetic acid (80:20:2 for cholesterol measurement and 90:10:1 for cholesterol ester measurement). Lipids were stained with phosphomolybdic acid and quantified using LAS1000 (Fuji film, Tokyo, Japan). Data were normalized against protein concentration.

Measurement of Cholesterol Esterification. Human skin fibroblasts were grown according to format 1. On day 3, cells were washed and the medium was replaced with 1 mL of medium C with and without LDL and 25-hydroxycholesterol in the presence and absence of inhibitors. After 24 h of incubation, each monolayer was labeled with 0.5 μCi [^{14}C]oleate. After 1 h incubation, cells were washed with PBS and were harvested using a rubber policeman. Then lipids were extracted (*35*) after protein measurement. Extracted lipids were applied to HPTLC plate (Merck) and developed in hexane/diethyl ether/glacial acetic acid (80:20:2). Radioactive lipids were quantified using BAS2500 (Fuji film, Tokyo, Japan), and the radioactivity was normalized against protein concentration. Cholesterol esterification in GM95 and Neuro-2a was measured in FCS-containing medium by adding 0.5 μCi [^{14}C]oleate for 1 h. The

incorporation of radioactivity to cholesteryl [^{14}C]oleate was determined as described above.

Streptolysin O Treatment. Human skin fibroblasts were grown on 24 well dishes for 3 days in the presence and absence of 10 μM D-PDMP. Cells were then washed with serum free medium followed by 10 min incubation on ice in the serum free medium containing various concentrations of streptolysin O. Viability of cells was measured using MTT assay (*36*).

Cytotoxicity of Paclitaxel. Neuro-2a cells were grown in 6 well dish in DMEM supplemented with 5% FCS for 1 day in the absence and presence of inhibitors. Then the medium was changed to paclitaxel containing medium with and without inhibitors, and cells were grown for 3 days. During incubation, the medium was changed to fresh medium with paclitaxel in the absence and presence of inhibitors every 24 h. After incubation, viability of cells was measured as described above (*36*).

Uptake of Fluorescent Paclitaxel. Neuro-2a cells were grown in DMEM supplemented with 5% FCS for 3 days in the absence and presence of inhibitors. Cells were then washed and further incubated for 1 h at 37 °C in phenol red free DMEM F12 with 5% FCS and 50 nM BODIPY FL paclitaxel in the absence and presence of inhibitors. The medium was then removed, followed by solubilization of cells in PBS containing 0.1% Triton X-100. 10% Triton X-100 solution was added to the removed medium so as to adjust the final detergent concentration to 0.1%. The fluorescence of both the medium and the cell suspension was measured with a fluorometer (JASCO, FP-6500) (λex = 505 nm, λem = 515 nm). When D-PDMP-treated cells were further treated with methyl-β-cyclodextrin (MβCD)/cholesterol complex, the cells were incubated for 30 min at 37 °C in DMEM with 5% FCS containing MβCD/cholesterol (final concentration of cholesterol, 100 μM). Cells were then washed and incubated with BODIPY FL paclitaxel in phenol red free DMEM F12 with 5% FCS for 1 h at 37 °C. Incorporation of fluorescent paclitaxel was measured as described above. MβCD/cholesterol was prepared as described (*37*).

RESULTS

D-PDMP and NB-DNJ but Not L-PDMP Inhibit the Metabolism of C6-NBD-Cer to C6-NBD-GlcCer. D-*threo*-1-Phenyl-2-decanoylamino-3-morpholino-1-propanol (D-PDMP) and *N*-butyl-deoxynojirimycin (*N*B-DNJ) are well-known inhibitors of UDP-glucose:ceramide glucosyltransferase (GCS). In contrast to D-PDMP, L-*threo*-1-phenyl-2-decanoylamino-3-morpholino-1-propanol (L-PDMP) does not inhibit GCS. We first confirmed that these inhibitors properly inhibit glycosphingolipid (GSL) synthesis in our experimental settings. 6-((*N*-(7-Nitrobenz-2-oxa-1,3-diazol-4-yl)amino)-hexanoyl)sphingosine (C6-NBD-Cer) is a useful ceramide analogue for measuring GSL synthesis in various cell types (*27*, *38*−*40*). When cells are incubated with C6-NBD-Cer, two major products, 6-((*N*-(7-nitrobenz-2-oxa-1,3-diazol-4-yl)amino)hexanoyl)sphingosine-1-phosphocholine (C6-NBD-sphingomyelin, C6-NBD-SM) and 6-((*N*-(7-nitrobenz-2-oxa-1,3-diazol-4-yl)amino)hexanoyl)sphingosine glucoside (C6-NBD-glucosylceramide, C6-NBD-GlcCer) are formed. In Figure 1, human skin fibroblasts were treated for 3 days with various inhibitors. C6-NBD-Cer was then added to the medium, and the lipids were extracted. The specimen gave three spots on the thin layer chromatogram, corresponding to C6-NBD-Cer, C6-NBD-glucosylceramide and C6-NBD-sphingomyelin. The relative fluorescence intensity is shown in Figure 1. As previously reported (*1*, *6*), D-PDMP and *N*B-DNJ inhibited the synthesis of C6-NBD-glucosylceramide. 5−10 μM D-PDMP was necessary to completely inhibit glucosylceramide synthesis whereas 50 times more *N*B-DNJ was required for the inhibition. Unlike D-PDMP, L-PDMP did not inhibit C6-NBD-glucosylceramide synthesis, but rather, the synthesis was slightly accelerated by the reagent as described (*41*). In the following study, 10 μM D- and L-PDMP and 500 μM *N*B-DNJ were employed in most of the cell experiments.

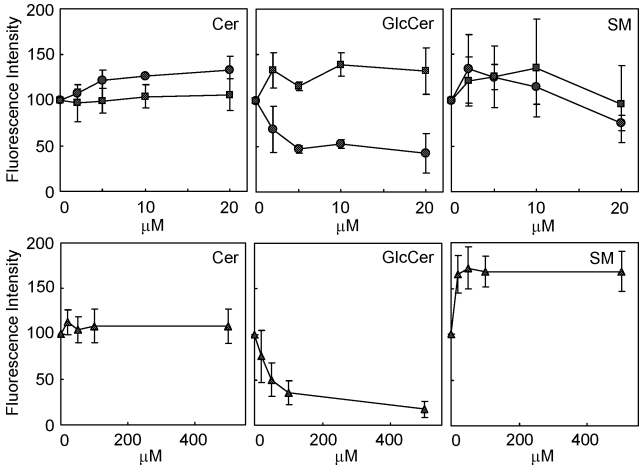

FIGURE 1: D-PDMP and *N*B-DNJ but not L-PDMP inhibit glycolipid synthesis. Human skin fibroblasts were incubated with various concentrations of D-PDMP (circle), L-PDMP (square), or *N*B-DNJ (triangle) for 3 days. C6-NBD-Cer was then added and the formation of C6-NBD-glucosylceramide and C6-NBD-sphingomyelin was measured as described in Materials and Methods. Data are mean of triplicate experiments ± SD. Cer, C6-NBD-Cer; GlcCer, C6-NBD-glucosylceramide; SM, C6-NBD-sphingomyelin.

D-PDMP Alters the Morphology of Bis(monoacylglycero)-phosphate (BMP)-Rich Membranes. Previously it was shown that PDMP induces vacuolization of late endosomes/lysosomes (*42*). The internal membranes of late endosomes are highly enriched with a unique negatively charged lipid, BMP (*18*−*20*). In Figure 2, we examined the morphology of BMP-containing membranes using the specific antibody that recognizes BMP (*18*). Immunofluorescence indicates that BMP-containing vesicles become enlarged during incubation with D-PDMP (Figure 2A−D). Electron microscopy revealed the accumulation of multilamellar structures in D-PDMP-treated cells (Figure 2G−I). These structures were labeled with anti-BMP antibody (Figure 2J). Our results indicate that D-PDMP alters the morphology of BMP-containing organelles.

D-PDMP Is Distributed in BMP-Containing Membranes. A fluorescent PDMP analogue is reported to accumulate in late endosomes/lysosomes (*42*, *43*). Hydrophobic amines such as D-PDMP are thought to pass through membranes, and, once accumulated in the acidic compartment, the amino group becomes positively charged and trapped inside the organelle. However, the intracellular distribution of non-fluorescent PDMP is not studied. In Figure 3, we investigated

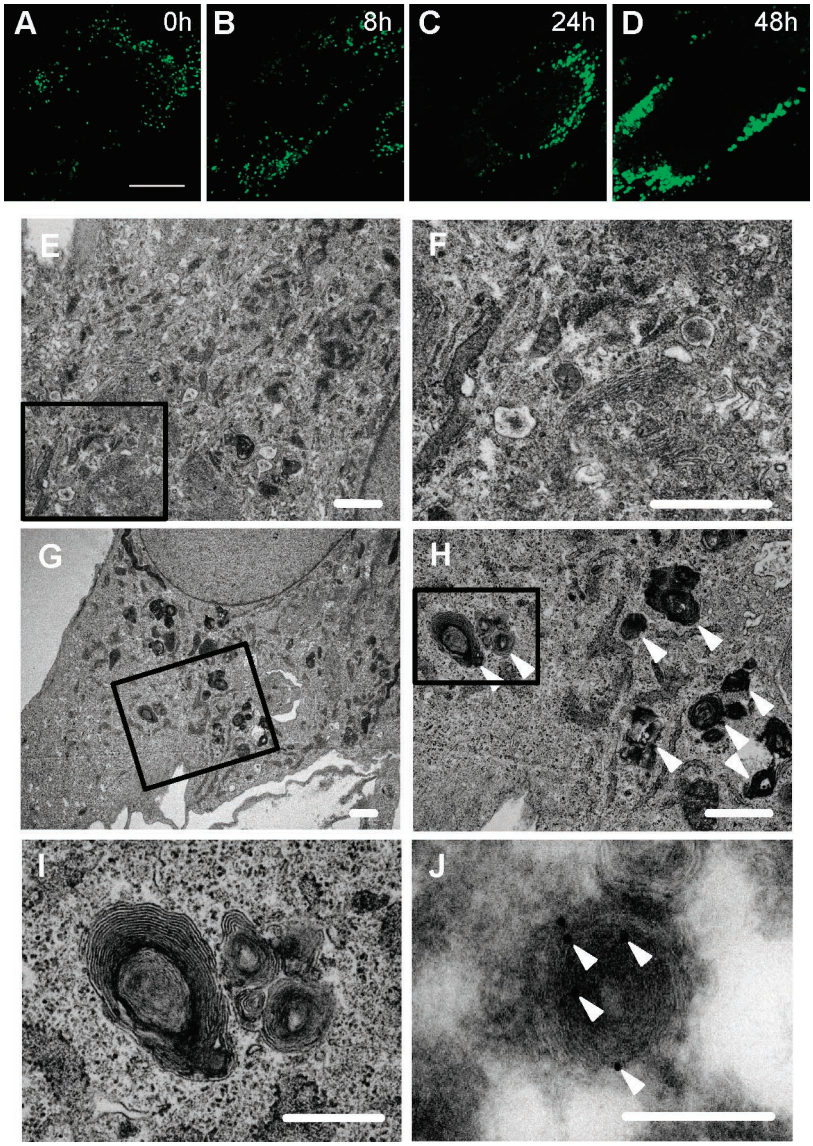

FIGURE 2: D-PDMP alters the morphology of BMP-containing organelle. (A−D) Human skin fibroblasts were grown in the presence of 10 μM D-PDMP. Cells were then fixed and labeled with anti-BMP antibody. Bar, 20 μm. (E−J) Electron micrographs of human skin fibroblasts grown for 2 days in the absence (E and F) or presence (G−J) of D-PDMP. E−I show conventional electron micrographs, J shows immunoelectron micrograph of BMP. F shows the higher magnification image from E, similarly, H from G, and I from H, respectively. Cell treated with D-PDMP had abundant multilamellar bodies (arrowheads in H), which were not seen in nontreated cells (E and F). The immunogold labeling (arrowheads in J) indicates that the multilamellar body contains BMP. Bars, E−H, 1 μm; I and J, 500 nm.

whether D-PDMP is accumulated in late endosomes by purifying the late endosome fraction from baby hamster kidney (BHK) cells in which the protocol for isolating late endosomes is well established (*18*, *28*). D-PDMP was detected by primuline staining after extraction and separation of lipids on thin-layer chromatography (TLC). The identity of D-PDMP was confirmed by measuring the mass spectrometry of the extracted spot (Figure 3). The ions were observed at *m*/*z* 391.38 ($[M + H]^+$) and 413.38 ($[M + Na]^+$), indicating that the detected spot is D-PDMP (calculated *m*/*z* values are 391.30 and 413. 28, respectively). From the primuline staining of standards we calculated that the BMP:PDMP ratio in the late endosome fraction is roughly 1:3. These results reveal that D-PDMP is distributed in late endosomes. However, our fractionation study shows that D-PDMP is also distributed in membranes other than late endosomes (data not shown), indicating that D-PDMP is not restricted in late endosomes. This is consistent with the observation that GCS is distributed in pre- and early Golgi apparatus (*44*).

D-PDMP Alters the Organization of BMP Membrane in a pH-Dependent Manner. The above results indicate that D-PDMP is distributed in BMP-containing membranes. BMP-rich membrane domain is suggested to be involved in membrane traffic from late endosomes as well as the degradation of sphingolipids in late endosomes/lysosomes (*17*, *21*, *22*). The disturbance of membrane traffic by BMP specific antibody suggests that the specific membrane organization of the lipid plays an important role in the function of BMP-rich membrane domains (*21*−*23*). BMP has a unique *sn*-1, *sn*-1′ stereoconfiguration, and fatty acids are esterified to unstable 2- and 2′-positions (*20*). In most mammalian cultured cells, the major molecular species is dioleoyl (diC18:1) BMP. We chemically synthesized naturally occurring 2,2′-dioleoyl *sn*-1, *sn*-1′-BMP (*23*, *29*) and examined the interaction between BMP and PDMP by

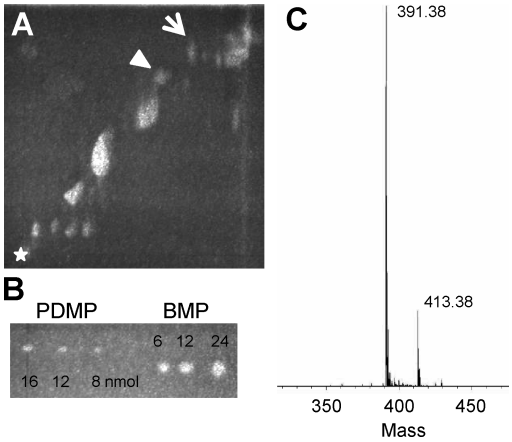

FIGURE 3: D-PDMP distributes in late endosomes. (A) Baby hamster kidney (BHK) cells were grown in the presence of 10 μM D-PDMP. After 24 h, late endosomal fractions were prepared as described in Materials and Methods. Lipids were then extracted and separated by two-dimensional chromatography. The arrow shows the position of D-PDMP whereas the arrowhead indicates BMP. The star points to the origin of the spot. (B) Different amounts of D-PDMP (PDMP) and BMP were developed on one-dimensional chromatography followed by primuline staining in order to obtain a calibration curve. (C) MALDI-TOF MS spectrum of the D-PDMP spot. The major peaks corresponds to $[M + H]^+$ at *m*/*z* 391.38 and $[M + Na]^+$ at *m*/*z* 413.38.

measuring small-angle X-ray scattering (Figure 4). We investigated the effect of pH to mimic the environment of the lumen of endosomes/lysosomes. BMP alone gave broad peaks at $q = \sim 0.90$ nm^{-1} and $q = \sim 1.50-1.90$ nm^{-1}, irrespective of the pH (Figure 4A−C). The peak at $q = 0.90$ nm^{-1} corresponds to the first order diffraction from a lamellar structure of BMP, while the peak at $q = \sim 1.50-1.90$ nm^{-1} is attributed to the bilayer form factor and the second order lamellar diffraction, indicating that BMP dispersion occurs in the swollen and loosely packed lamellar structures. The addition of D-PDMP at low pH dramatically changes this scattering pattern. At 1 mM D-PDMP, the intensity of the broad peak at $q = \sim 0.90$ nm^{-1} was decreased and a sharp diffraction appeared at $q = 1.30$ nm^{-1}. At 2.5 mM D-PDMP, the diffraction peaks were shifted to the wide-angle region and clear first and second order diffractions corresponding to a repeat distance $d = 4.58$ nm were observed, indicating that D-PDMP induced a closely packed multilamellar ordering of the membrane (Figure 4A). Since another set of first and second order diffractions corresponding to a repeat distance of 6.10 nm was observed at 2.5 mM D-PDMP concentration, initial lamellar structures with a large repeat distance coexisted in a phase separated manner with the closely packed lamellar structures. This effect was pH-dependent and D-PDMP did not significantly alter the scattering pattern at neutral and alkaline pH (Figure 4B,C). We also examined the effects of L-PDMP and *N*B-DNJ (Figure 4D,E). L-PDMP altered the scattering pattern of BMP as D-PDMP did (Figure 4D) whereas *N*B-DNJ did not affect the scattering profile (Figure 4E). D- and L-PDMP and *N*B-DNJ by themselves yielded no profile in small-angle scattering under the present conditions (data not shown). Figure 4F−H shows that the light scattering profile of D-PDMP changed in a pH-dependent manner. At neutral and alkaline pH, D-PDMP forms large micelles whereas the size of the micelle is much smaller at low pH, suggesting the different packaging of the molecule at low pH. This alteration of the organization of D-PDMP itself may be the cause of the alteration of BMP membrane by the drug at low pH.

D-PDMP Inhibits the Activation of Lysosomal Acid Lipase by BMP. The above results suggest that D-PDMP is accumulated in late endosomes and interacts with BMP. The scattering profile suggests that D-PDMP covers the negative charge of BMP under low pH conditions (*45*). It is known that acid lipase requires certain negatively charged phospholipids for maximum activity (*46*). BMP comprises more than 50% of phospholipids in the internal membrane domains of late endosomes and thus a major source of negatively charged phospholipids there (*20*). Figure 5 indicates that the lysosomal acid lipase activity was enhanced by the addition of BMP and D-PDMP inhibited this enhancement in dose-dependent manner. The basal acid lipase activity was not affected by D-PDMP, suggesting that D-PDMP does not directly inhibit the enzyme. These results thus suggest that D-PDMP modifies the organization of late endosome/lysosome specific lipids and thus inhibits acid lipase activity of the organelle.

D-PDMP and L-PDMP but Not NB-DNJ Inhibit Hydrolysis of [Cholesteryl-4-^{14}C] Oleate-Containing LDL and Increase the Cellular Cholesterol Ester Content. Acid lipase is involved in the degradation of low-density lipoproteins (LDL). In Figure 6, we investigated the effect of D-PDMP on LDL uptake and LDL-cholesteryl ester hydrolysis in human skin fibroblasts. Figure 6A shows the incorporation of cholesteryl BODIPY FL C12-containing LDL in the absence and presence of 10 μM D-PDMP. The fluorescence image shows that D-PDMP enhanced the uptake of LDL. In contrast, the presence of D-PDMP dramatically inhibited the degradation of [cholesteryl-4-^{14}C] oleate-containing LDL (Figure 6B). L-PDMP also inhibited the degradation while *N*B-DNJ showed little effect on the degradation of [cholesteryl-4-^{14}C] oleate (Figure 6C). The cellular content of cholesterol ester was then measured after treatment with D-PDMP, L-PDMP, and *N*B-DNJ (Figure 6D). Cholesterol ester content was significantly increased when cells were incubated with D-PDMP and L-PDMP. In contrast, *N*B-DNJ did not affect the cellular level of cholesterol esters. Intracellular accumulation of cholesterol esters was also examined by staining cells with nile red, which stains neutral lipids (*47*) (Figure 7). Nile red stained the Golgi apparatus in control cells. After treating cells with D-PDMP and L-PDMP, nile red fluorescence was enhanced and partially colocalized with CD63, a protein which has four membrane spanning domains and which localizes in late endosomes (*20*, *48*, *49*), indicating late endosome/lysosome accumulation of neutral lipids. Figure 7 shows that the shape of late endosome changed from small dots to large vacuoles upon treatment with D- and L-PDMP as observed in Figure 2. *N*B-DNJ did not significantly affect the distribution of nile red labeling. Our results indicate that D-PDMP and L-PDMP but not *N*B-DNJ inhibit the degradation of LDL.

D-PDMP and L-PDMP but Not NB-DNJ Inhibit Cholesterol Esterification. We then measured the effect of D-PDMP on low-density lipoprotein (LDL)-stimulated cholesterol esterification. In Figure 8A, human skin fibroblasts were incubated in medium C containing varying concentrations of LDL in the absence and presence of 10 μM D-PDMP. D-PDMP strongly inhibited LDL-induced cholesteryl ester formation. We included mevinolin, a potent inhibitor of

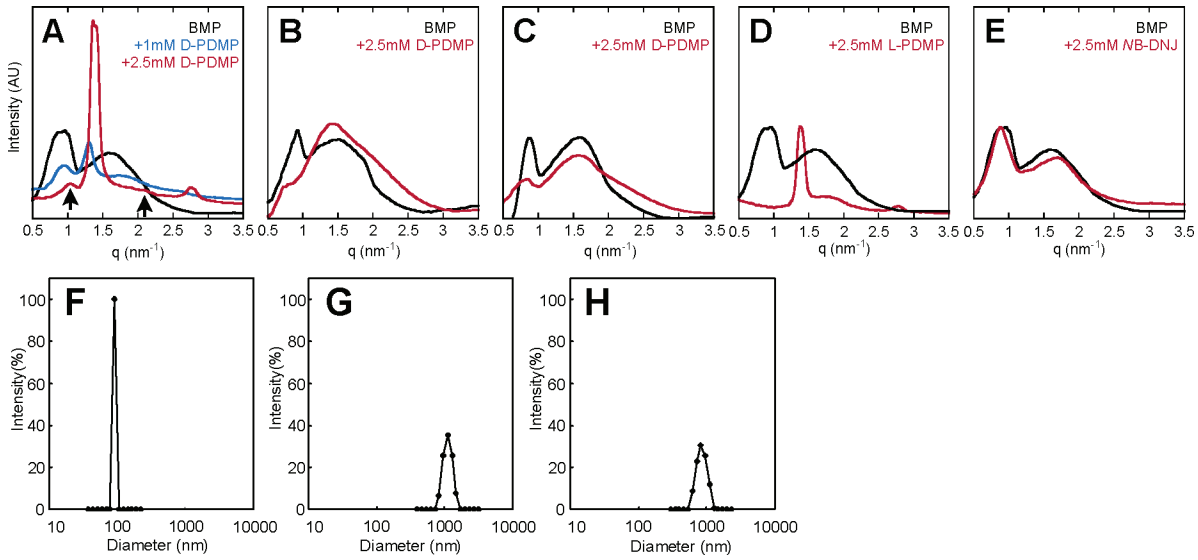

FIGURE 4: D-PDMP modifies the organization of BMP membranes. (A−E) Small-angle X-ray scattering (SAXS) profiles of BMP dispersions containing various inhibitors. A−C, BMP dispersions were mixed with D-PDMP in 200 mM sodium citrate buffer at pH 4.6 (A), in 20 mM HEPES buffer containing 150 mM NaCl at pH 7.5 (B), and in 20 mM tricine buffer containing 150 mM NaCl at pH 8.5 (C). In D and E, effects of L-PDMP (D) and *N*B-DNJ (E) on BMP dispersions in sodium citrate buffer at pH 4.6 are shown. The arrows in A indicate the first and second order diffraction peaks corresponding to a lamellar repeat distance of 6.10 nm. The addition of D-PDMP changed the SAXS pattern of BMP dispersions significantly so as to display clear sharp diffractions, characteristic of closely stacked multilamellar structures. (F−H) The average hydrodynamic diameter of PDMP aggregate investigated by DLS at pH 4.6 (F), 7.4 (G), and 8.5 (H). The buffers used for respective pH conditions were the same as those employed in X-ray experiments. At pH 4.6, PDMP formed a highly monodisperse micellar aggregate with an average hydrodynamic diameter of ~90 nm, while at pH 7.4 and 8.5 it formed a polydisperse large aggregate with an average diameter of ~800−1000 nm.

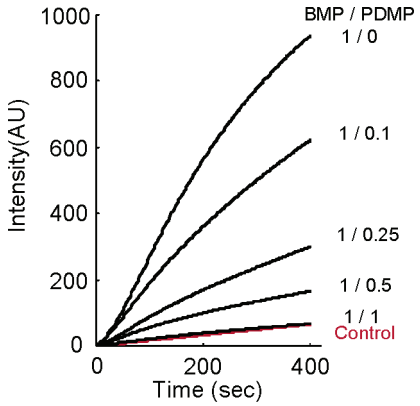

FIGURE 5: D-PDMP inhibits the enhancement of acid lipase activity by BMP. Acid lipase activity of homogenates from human skin fibroblasts was measured in the absence and presence of BMP dispersions containing various molar ratios of D-PDMP. Control shows the enzyme activity in the absence of BMP.

mevalonate synthesis, in the medium. Thus, the observed results were not due to impaired cholesterol biosynthesis in D-PDMP-treated cells. We then examined the effect of various inhibitors on LDL-stimulated cholesterol esterification (Figure 8B). Whereas esterification was inhibited by D- and L-PDMP as well as U18666A (*50*−*52*), a well-characterized hydrophobic amine which specifically inhibits cholesterol traffic from late endosomes/lysosomes, *N*B-DNJ did not inhibit LDL-induced cholesteryl ester formation. Instead, cholesterol esterification was slightly stimulated by *N*B-DNJ treatment. Cellular cholesterol esterification is also stimulated when cells are incubated with oxygenated sterols such as 25-hydroxycholesterol (*53*). In Figure 8C, we measured 25-hydroxycholesterol-stimulated cholesterol esterification in mevinolin-treated human skin fibroblasts incubated in the absence and presence of inhibitors. Again D- and L-PDMP significantly inhibited esterification. U18666A partially inhibited 25-hydroxycholesterol-induced cholesterol esterification whereas *N*B-DNJ did not affect the cholesterol esterification.

GM95 cells have a defect in the first step of GSL synthesis that is catalyzed by UDP-glucose:N-acylsphingosine glucosyltransferase, thus, they are entirely lacking GSLs (*24*). After cells were treated with 10 μM D-PDMP in the growth medium for 3 days, cholesterol esterification was measured by adding [^{14}C]oleate (Figure 8D). The esterification was inhibited, as has been observed in human skin fibroblasts. This result indicates that D-PDMP alters cholesterol metabolism in a GSL-independent manner.

D-PDMP Alters Intracellular Distribution of Free Cholesterol. In Figure 9A, human skin fibroblasts were treated with 10 μM D-PDMP for 3 days. Cells were then fixed, permeabilized, and labeled with a cholesterol probe, filipin (*54*, *55*). D-PDMP treatment resulted in accumulated intracellular cholesterol. Accumulation of cholesterol was also observed when cells were treated with L-PDMP. In Figure 9B, cholesterol distribution was compared with BMP. The partial colocalization observed indicates that D-PDMP accumulates cholesterol in late endosomes/lysosomes. In Figure 9C, human skin fibroblasts were grown in the presence of various concentrations of D-PDMP and the cholesterol content was determined. Although D-PDMP accumulated cholesterol intracellularly, the content of cholesterol was not significantly altered by D-PDMP. Streptolysin O is a bacterial toxin that kills cells in a cholesterol-dependent manner (*40*, *56*). Thus the sensitivity of cells to this toxin closely reflects the amount of cell surface cholesterol. In Figure 9D, cells were grown in the presence and absence of 10 μM D-PDMP for 3 days and the sensitivity of cells to streptolysin O was measured. Cells became slightly but significantly resistant

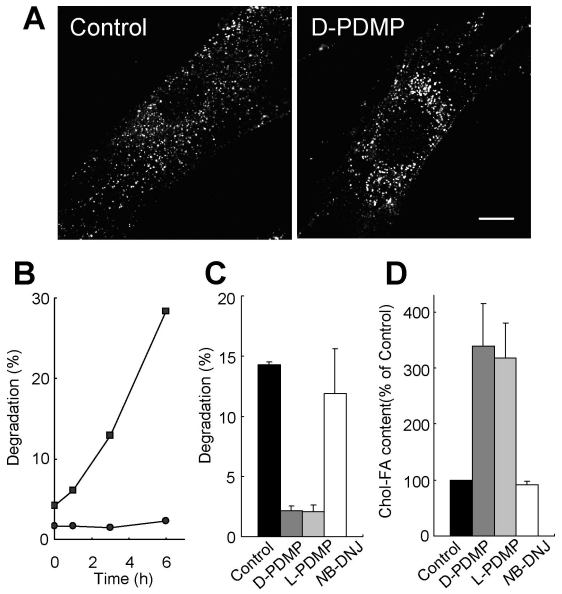

FIGURE 6: D-PDMP and L-PDMP but not *N*B-DNJ inhibit hydrolysis of [cholesteryl-4-^{14}C] oleate-containing LDL. (A) Uptake of reconstituted LDL in the absence (control) and the presence of 10 μM D-PDMP (D-PDMP). Incorporation of BODIPY FL C12-containing LDL was measured as described in Materials and Methods. (B, C) Hydrolysis of [cholesteryl-4-^{14}C] oleate-containing LDL was quantified as described in Materials and Methods. (B) Time course of degradation. Squares show the results in the absence of D-PDMP whereas circles indicate the degradation in the presence of 10 μM D-PDMP. (C) The effects of various drugs on the degradation of [cholesteryl-4-^{14}C] oleate-containing LDL were measured after 6 h incubation. Control, without inhibitor; D-PDMP, 10 μM D-PDMP; L-PDMP, 10 μM L-PDMP; *N*B-DNJ, 500 μM *N*B-DNJ. Data are mean of triplicate experiments ± SD. (D) Human skin fibroblasts were grown in the presence and absence of inhibitors for 3 days. Lipids were extracted and separated on TLC, and the content of cholesterol ester was measured as described in Materials and Methods. Control, without inhibitor; D-PDMP, 10 μM D-PDMP; L-PDMP, 10 μM L-PDMP; *N*B-DNJ, 500 μM *N*B-DNJ. Data are mean of triplicate experiments ± SD.

to the toxin, indicating that cell surface cholesterol had been decreased by the D-PDMP treatment. Our results indicate that D-PDMP alters the cellular distribution of cholesterol but does not significantly affect cholesterol content.

PDMP Modulates the Transport of Paclitaxel in Neuroblastoma Cells in a Cholesterol-Dependent Manner. The above results indicate that D-PDMP inhibits the degradation of LDL, and this leads to an inhibition of cholesterol esterification and a decrease of cell surface cholesterol. It is suggested that P-glycoprotein is associated with raft-like membrane domains and cholesterol modulates P-glycoprotein activity (*57*, *58*). We investigated whether the MDR cell chemosensitization effect of PDMP is related to the alteration of cholesterol homeostasis caused by PDMP. It is reported that PDMP chemosensitizes Neuro-2a cells to paclitaxel (*7*). Figure 10A shows that both D- and L-PDMP chemosensitize Neuro-2a cells whereas *N*B-DNJ is without effect. Similar to the result in human skin fibroblasts and melanoma mutants, D-PDMP inhibited cholesterol esterification and accumulated cholesterol ester in Neuro-2a cells (Figure 10B). In Figure 10C, we show the uptake of fluorescent paclitaxel in cells treated with various inhibitors. D-PDMP increased the uptake of BODIPY FL paclitaxel almost 2-fold. This result agrees with a previous observation that PDMP decreases the efflux of paclitaxel. The increased uptake of

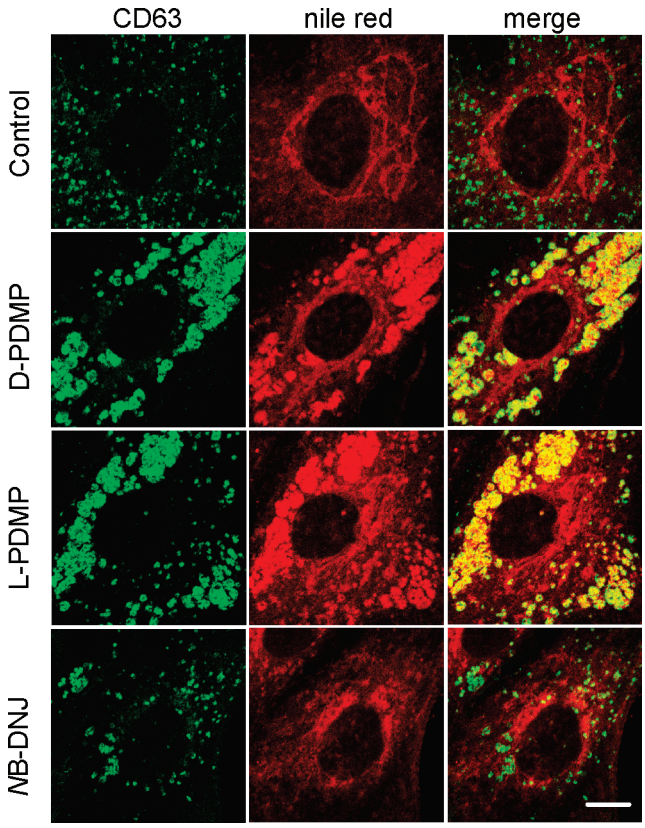

FIGURE 7: D-PDMP accumulates neutral lipids in late endosomes. Human skin fibroblasts were incubated with 10 μM of D-PDMP, L-PDMP, and 100 μM *N*B-DNJ for 3 days. Cells were fixed and doubly labeled with nile red and anti-CD63 antibody. Bar, 10 μm.

fluorescent paclitaxel was also observed in L-PDMP-treated cells. In contrast to D- and L-PDMP, *N*B-DNJ did not affect the uptake of fluorescent paclitaxel in Neuro-2a cells. These results indicate that inhibition of GCS does not correlate with the enhanced uptake of fluorescent paclitaxel. When D-PDMP-treated cells were further incubated with a methyl-β-cyclodextrin (MβCD)/cholesterol complex, the uptake was suppressed to a level below that in the absence of inhibitors. MβCD/cholesterol treatment is known to increase cellular cholesterol. These results therefore suggest that PDMP modulates transport of paclitaxel in neuroblastoma cells in a cholesterol-dependent manner.

DISCUSSION

In the present study, we showed that, in addition to the inhibitory effect on GCS, D-PDMP accumulates in late endosomes and modifies the organization of BMP-containing membranes. This results in an inhibition of the degradation of lipoproteins and an alteration of cellular cholesterol homeostasis, including a decrease in the cell surface cholesterol, that modifies the transport of anticancer reagents. These effects are independent of the inhibition of GCS.

Inhibition of acid lipase activity resembles Wolman disease, a late endosomal/lysosomal acid lipase deficiency (*59*). In Wolman disease, complete deficiency of acid lipase leads to massive accumulation of lysosomal cholesteryl esters. Defective release of free cholesterol from late endosomes/lysosomes inhibits LDL-dependent cholesterol esterification as observed in D-PDMP treated cells.

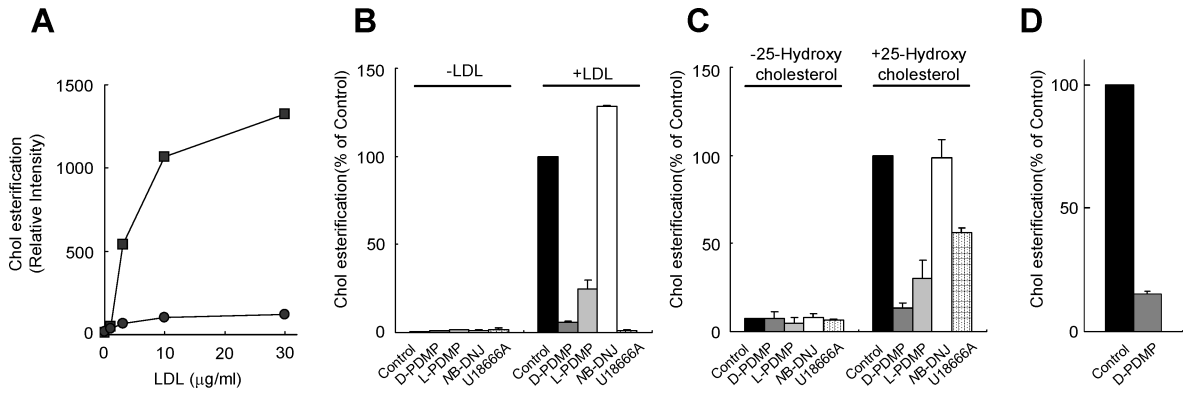

FIGURE 8: D-PDMP and L-PDMP but not *N*B-DNJ inhibit cholesterol esterification. (A) Effect of the concentration of LDL on cholesterol esterification in the presence (circle) and absence (square) of 10 μM PDMP. The incorporation of radioactivity to cholesteryl [^{14}C]oleate was determined as described in Materials and Methods. Each data point represents the average of two wells. (B) Effects of various inhibitors on LDL-stimulated cholesterol esterification. Control, without inhibitor; D-PDMP, 10 μM D-PDMP; L-PDMP, 10 μM L-PDMP; *N*B-DNJ, 500 μM *N*B-DNJ; U18666A, 1 μg/mL U18666A. Each data point represents the average of two wells. (C) Effects of various inhibitors on 25-hydroxycholesterol-stimulated cholesterol esterification. Control, without inhibitor; D-PDMP, 10 μM D-PDMP; L-PDMP, 10 μM L-PDMP; *N*B-DNJ, 500 μM *N*B-DNJ; U18666A, 1 μg/mL U18666A. Each data point represents the average of two wells. (D) GM95 cells were incubated with and without 10 μM D-PDMP in the growth medium for 3 days followed by the addition of [^{14}C]oleic acid. After 1 h incubation, the incorporation of radioactivity to cholesterol ester was measured as described in Materials and Methods.

D-PDMP Alters Cholesterol Homeostasis in a Glycolipid-Independent Manner. D-PDMP is a well-recognized inhibitor of GCS (*1*, *2*). However, apart from its effect on sphingolipid synthesis, PDMP is reported to also have other activities. These include (i) inhibition of other enzymes involved in glycolipid metabolism (*60*−*62*), (ii) cell cycle arrest (*63*), (iii) inhibition of membrane traffic from the Golgi apparatus (*43*, *64*), (iv) induction of lysosome vacuolization (*42*), and (v) accumulation of intracellular cholesterol (*12*, *13*). Roff et al. (*12*) report the inhibition of cholesteryl ester formation and lysosomal cholesterol accumulation by PDMP (RV-538). Intracellular accumulation of a fluorescent PDMP analogue is also reported (*42*, *43*). They hypothesized that PDMP and other hydrophobic amines such as U18666A share a common mechanism to inhibit cholesteryl ester formation and cholesterol accumulation. Inokuchi et al. (*13*) hypothesize that the accumulation of cholesterol by D-PDMP is a result of a trapping of cholesterol within GSL-laden compartments due to physical association of cholesterol with GSLs. We have shown that D-PDMP accumulates in late endosomes and modifies the structure of the BMP-containing membrane, leading to inhibition of the degradation of LDL and thus an altered cellular cholesterol homeostasis. This effect was observed with L-PDMP, which does not inhibit GCS. Inhibition of cholesterol esterification was also observed in a glycolipid-null melanoma mutant. These results indicate that D-PDMP alters cellular cholesterol homeostasis in a glycolipid-independent manner.

D-PDMP Modulates the Transport of Anticancer Reagents by Altering Cellular Cholesterol Homeostasis. D-PDMP is able to sensitize MDR cells (*3*−*8*). A major cause of MDR is the activation of P-glycoprotein (*65*, *66*). P-glycoprotein is a member of the ATP-binding-casette (ABC) transporter superfamily and acts as an ATP-dependent efflux pump against a broad range of anticancer reagents. The lipid environment influences the ATPase activity of P-glycoprotein (*57*, *58*, *67*−*69*). Modok et al. (*57*) showed that P-glycoprotein retains function in liquid-ordered cholesterol and sphingolipid model membranes. Gayet et al. (*69*) showed that cholesterol increases with the level of chemoresistance of the human CEM acute lymphoblastic leukemia. They suggest that cholesterol is involved in the P-glycoprotein-induced MDR phenotype and controls both the ATPase and drug efflux activities of P-glycoprotein. Our results indicated that D-PDMP inhibits the degradation of LDL and decreases cell surface cholesterol. Concomitantly, the uptake of fluorescent paclitaxel was increased in Neuro-2a cells, suggesting an inhibition of P-glycoprotein activity. The reversal of drug uptake by MβCD/cholesterol treatment suggests that D-PDMP modulates P-glycoprotein activity mainly by altering the distribution of cell surface cholesterol. It is reported that progesterone, but not U18666A, inhibits P-glycoprotein activity (*52*). Progesterone is reported to inhibit cholesterol transport from the plasma membrane to ER (*70*).

Role of GCS in the MDR Phenotype. A role for GCS in the MDR phenotype is supported by following observations: (i) There are elevated levels of glycolipids and the MDR phenotype correlate in some cancer cells (*4*, *71*−*73*). (ii) Overexpression of GCS enhances the drug resistance of MCF-7 breast cancer cells (*74*, *75*). (iii) D-PDMP and its derivatives are able to sensitize drug-resistant cancer cells (*3*−*9*). Recently Veldman et al. (*76*) reported that a GCS-deficient melanoma mutant and a GCS transfectant showed similar sensitivity to anticancer reagents. It has also been shown that the GCS inhibitors *N*N-DGJ and *N*B-DGJ do not chemosensitize MDR cells whereas D-PDMP does under the same conditions. It was concluded that the chemosensitization achieved by D-PDMP cannot be caused by an inhibition of GCS alone (*11*). Our results suggest that D-PDMP chemosensitizes cells by altering cellular cholesterol. D-PDMP is reported to accumulate ceramide in certain cell types (*1*, *7*, *62*). It is thus possible that ceramide-dependent signals are involved in D-PDMP-dependent chemosensitization. However, we consider this unlikely since (i) L-PDMP, which does not inhibit GCS, behaves similarly to D-PDMP; (ii) alteration of cholesterol homeostasis was observed even in GCS-deficient GM95 melanoma cells; and (iii) the effect of D-PDMP was reversed by 30 min treatment with MβCD/cholesterol. Such results suggest that D-PDMP chemosensitizes cancer cells in a glycolipid-independent manner.

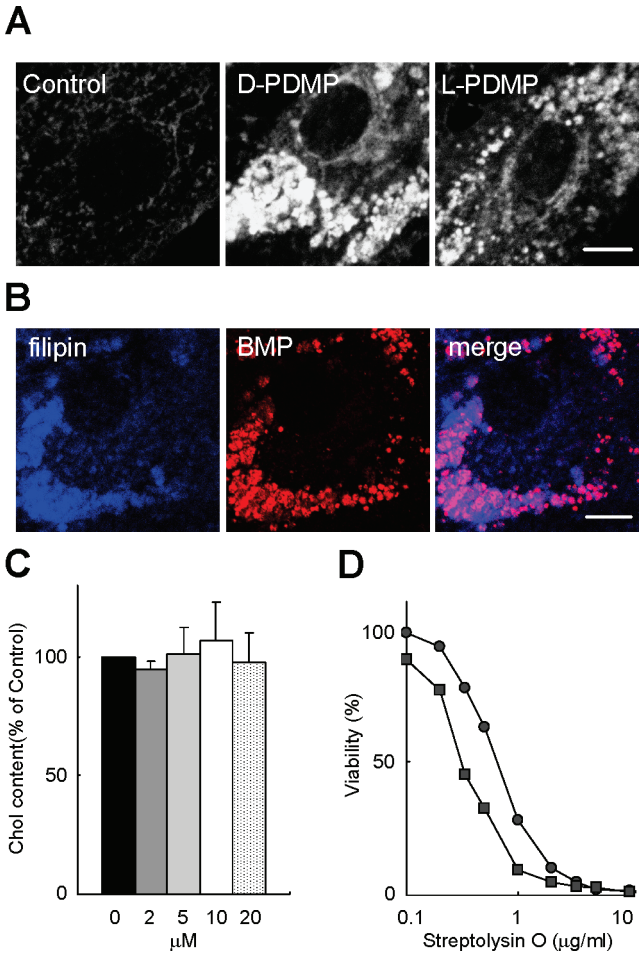

FIGURE 9: D-PDMP alters intracellular distribution of cholesterol. (A) Human skin fibroblasts were incubated with 10 μM D- or L-PDMP for 3 days. Cells were then fixed and labeled with filipin as described in Materials and Methods. Bar, 10 μm. (B) Human skin fibroblasts were treated with 10 μM D-PDMP for 3 days. Cells were then fixed and doubly labeled with anti-bis(monoacylglycero)-phosphate (BMP) antibody and filipin. Bar, 10 μm. (C) Human skin fibroblasts were grown in the presence of various concentrations of D-PDMP for 3 days. Lipids were extracted and separated on TLC, and free cholesterol was measured as described in Materials and Methods. Data are mean of triplicate experiments ± SD. (D) Human skin fibroblasts were incubated for 3 days in the presence (circle) and absence (square) of 10 μM D-PDMP. Sensitivity of cells to streptolysin O was measured as described in Materials and Methods. The data are representative results of four independent experiments. The decreased sensitivity of D-PDMP-treated cells indicated that cell surface cholesterol was decreased by the drug treatment.

The BMP Domain: A General Target for Hydrophobic Amines? It has been demonstrated that certain hydrophobic amines alter cellular cholesterol homeostasis (*50*, *51*). However the mechanism(s) for this effect have not been well characterized. Our results suggest that one target of these compounds is late endosome/lysosome specific lipids. BMP comprises less than 1% of the total phospholipids in most cells. However, the content is increased to 15% in late endosomes (*18*). In the specific internal membrane domains, this lipid occupies more than 70% of the total phospholipids (*20*). Using specific antibody, the role of this membrane domain in the protein and lipid trafficking from late endosomes have been reported (*21*, *22*). BMP is also a cofactor of several sphingolipid degradation complexes in late endosomes/lysosomes (*17*). The results reported here

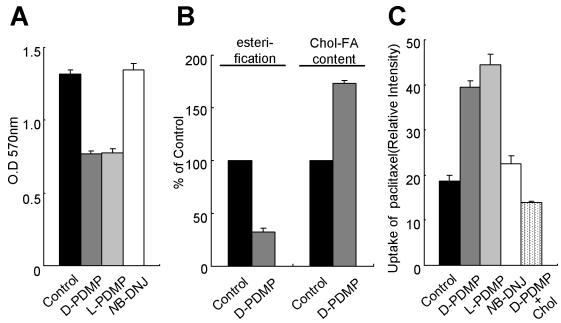

FIGURE 10: PDMP modifies the uptake of fluorescent paclitaxel in a cholesterol-dependent manner. (A) Neuro-2a cells were treated with paclitaxel in the absence and presence of various inhibitors as described in Materials and Methods. The viability was measured using the MTT assay. (B) Neuro-2a cells were incubated with and without 10 μM D-PDMP in the growth medium for 3 days followed by the addition of [^{14}C]oleic acid. After 1 h incubation, the incorporation of radioactivity to cholesterol ester was measured as described in Materials and Methods (esterification). Neuro-2a cells were grown as described above. The content of cholesterol ester was then measured as described in Materials and Methods (Chol-FA content). Data are mean of triplicate experiments ± SD. (C) Neuro-2a cells were pretreated with various inhibitors, and the uptake of BODIPY FL paclitaxel was measured as described in Materials and Methods. Control, without inhibitor; D-PDMP, 10 μM D-PDMP; L-PDMP, 10 μM L-PDMP; *N*B-DNJ, 500 μM *N*B-DNJ; D-PDMP + Chol, D-PDMP (10 μM) followed by MβCD/cholesterol treatment. Data are mean of triplicate experiments ± SD.

indicate that D-PDMP modifies the organization of this lipid and thus alters the function of the membrane domains. The specific mechanism of the effect on the function of the membrane domains will be the subject of future studies.

ACKNOWLEDGMENT

We are grateful to A. Yamaji-Hasegawa, H. Shogomori, F. Hullin-Matsuda, K. Iwamoto, M. Takahashi, M. Abe, and K. Murase for critically reading the manuscript and A. Suzuki for his support throughout the experiments. We thank K. Shibata for his technical help in SAXS measurements at SPring-8.

REFERENCES

1. Radin, N. S., Shayman, J. A., and Inokuchi, J. (1993) Metabolic effects of inhibiting glucosylceramide synthesis with PDMP and other substances, *Adv. Lipid Res. 26*, 183−213.
2. Sillence, D. J., Puri, V., Marks, D. L., Butters, T. D., Dwek, R. A., Pagano, R. E., and Platt, F. M. (2002) Glucosylceramide modulates membrane traffic along the endocytic pathway, *J. Lipid Res. 43*, 1837−45.
3. Lavie, Y., Cao, H., Volner, A., Lucci, A., Han, T. Y., Geffen, V., Giuliano, A. E., and Cabot, M. C. (1997) Agents that reverse multidrug resistance, tamoxifen, verapamil, and cyclosporin A, block glycosphingolipid metabolism by inhibiting ceramide glycosylation in human cancer cells, *J. Biol. Chem. 272*, 1682−7.
4. Morjani, H., Aouali, N., Belhoussine, R., Veldman, R. J., Levade, T., and Manfait, M. (2001) Elevation of glucosylceramide in multidrug-resistant cancer cells and accumulation in cytoplasmic droplets, *Int. J. Cancer 94*, 157−65.
5. Olshefski, R. S., and Ladisch, S. (2001) Glucosylceramide synthase inhibition enhances vincristine-induced cytotoxicity, *Int. J. Cancer 93*, 131−8.
6. Radin, N. S. (2003) Killing tumours by ceramide-induced apoptosis: a critique of available drugs, *Biochem. J. 371*, 243−56.
7. Sietsma, H., Veldman, R. J., Kolk, D., Ausema, B., Nijhof, W., Kamps, W., Vellenga, E., and Kok, J. W. (2000) 1-phenyl-2-

decanoylamino-3-morpholino-1-propanol chemosensitizes neuroblastoma cells for taxol and vincristine, *Clin. Cancer Res. 6*, 942−8.
8. Shabbits, J. A., and Mayer, L. D. (2002) P-glycoprotein modulates ceramide-mediated sensitivity of human breast cancer cells to tubulin-binding anticancer drugs, *Mol. Cancer Ther. 1*, 205−13.
9. Gouaze, V., Liu, Y. Y., Prickett, C. S., Yu, J. Y., Giuliano, A. E., and Cabot, M. C. (2005) Glucosylceramide synthase blockade down-regulates P-glycoprotein and resensitizes multidrug-resistant breast cancer cells to anticancer drugs, *Cancer Res. 65*, 3861−67.
10. Glaros, E. N., Kim, W. S., Quinn, C. M., Wong, J., Gelissen, I., Jessup, W., and Garner, B. (2005) Glycosphingolipid accumulation inhibits cholesterol efflux via the ABCA1/apolipoprotein A-I pathway: 1-phenyl-2-decanoylamino-3-morpholino-1-propanol is a novel cholesterol efflux accelerator, *J. Biol. Chem. 280*, 24515−23.
11. Norris-Cervetto, E., Callaghan, R., Platt, F. M., Dwek, R. A., and Butters, T. D. (2004) Inhibition of glucosylceramide synthase does not reverse drug resistance in cancer cells, *J. Biol. Chem. 279*, 40412−8.
12. Roff, C. F., Goldin, E., Comly, M. E., Cooney, A., Brown, A., Vanier, M. T., Miller, S. P., Brady, R. O., and Pentchev, P. G. (1991) Type C Niemann-Pick disease: use of hydrophobic amines to study defective cholesterol transport, *Dev. Neurosci. 13*, 315−9.
13. Inokuchi, J. I., Uemura, S., Kabayama, K., and Igarashi, Y. (2000) Glycosphingolipid deficiency affects functional microdomain formation in Lewis lung carcinoma cells, *Glycoconjugate J. 17*, 239−45.
14. Nagafuku, M., Kabayama, K., Oka, D., Kato, A., Tani-ichi, S., Shimada, Y., Ohno-Iwashita, Y., Yamasaki, S., Saito, T., Iwabuchi, K., Hamaoka, T., Inokuchi, J., and Kosugi, A. (2003) Reduction of glycosphingolipid levels in lipid rafts affects the expression state and function of glycosylphosphatidylinositol-anchored proteins but does not impair signal transduction via the T cell receptor, *J. Biol. Chem. 278*, 51920−7.
15. Kobayashi, T., Gu, F., and Gruenberg, J. (1998) Lipids, lipid domains and lipid-protein interactions in endocytic membrane traffic, *Semin. Cell Dev. Biol. 9*, 517−26.
16. Gruenberg, J. (2001) The endocytic pathway: a mosaic of domains, *Nat. Rev. Mol. Cell Biol. 2*, 721−30.
17. Kolter, T., and Sandhoff, K. (2005) Principles of Lysosomal Membrane Digestion-Stimulation of Sphingolipid Degradation by Sphingolipid Activator Proteins and Anionic Lysosomal Lipids, *Annu. Rev. Cell Dev. Biol. 21*, 81−103.
18. Kobayashi, T., Stang, E., Fang, K. S., de Moerloose, P., Parton, R. G., and Gruenberg, J. (1998) A lipid associated with the antiphospholipid syndrome regulates endosome structure and function, *Nature 392*, 193−7.
19. Kobayashi, T., Yamaji-Hasegawa, A., and Kiyokawa, E. (2001) Lipid domains in the endocytic pathway, *Semin. Cell Dev. Biol. 12*, 173−82.
20. Kobayashi, T., Beuchat, M. H., Chevallier, J., Makino, A., Mayran, N., Escola, J. M., Lebrand, C., Cosson, P., and Gruenberg, J. (2002) Separation and characterization of late endosomal membrane domains, *J. Biol. Chem. 277*, 32157−64.
21. Kobayashi, T., Beuchat, M. H., Lindsay, M., Frias, S., Palmiter, R. D., Sakuraba, H., Parton, R. G., and Gruenberg, J. (1999) Late endosomal membranes rich in lysobisphosphatidic acid regulate cholesterol transport, *Nat. Cell Biol. 1*, 113−8.
22. Le Blanc, I., Luyet, P. P., Pons, V., Ferguson, C., Emans, N., Petiot, A., Mayran, N., Demaurex, N., Faure, J., Sadoul, R., Parton, R. G., and Gruenberg, J. (2005) Endosome-to-cytosol transport of viral nucleocapsids, *Nat. Cell Biol. 7*, 653−64, Epub 2005 Jun 12.
23. Matsuo, H., Chevallier, J., Mayran, N., Le Blanc, I., Ferguson, C., Faure, J., Satori Blanc, N., Matile, S., Dubochet, J., Sadoul, R., Parton, R. G., Vilois, F., and Gruenberg, J. (2004) Role of LBPA and Alix in multivesicular liposome formation and endosome organization, *Science 303*, 531−4.
24. Ichikawa, S., Nakajo, N., Sakiyama, H., and Hirabayashi, Y. (1994) A mouse B16 melanoma mutant deficient in glycolipids, *Proc. Natl. Acad. Sci. U.S.A. 91*, 2703−7.
25. Faust, J. R., Goldstein, J. L., and Brown, M. S. (1977) Receptor-mediated uptake of low-density lipoprotein and utilization of its cholesterol for steroid synthesis in cultured mouse adrenal cells, *J. Biol. Chem. 252*, 4861−71.
26. Sleight, R. G., and Pagano, R. E. (1983) Rapid appearance of newly synthesized phosphatidylethanolamine at the plasma membrane, *J. Biol. Chem. 258*, 9050−8.
27. Kobayashi, T., and Pagano, R. E. (1989) Lipid transport during mitosis. Alternative pathways for delivery of newly synthesized lipids to the cell surface, *J. Biol. Chem. 264*, 5966−73.
28. Gorvel, J. P., Chavrier, P., Zerial, M., and Gruenberg, J. (1991) rab5 controls early endosome fusion in vitro, *Cell 64*, 915−25.
29. Chevallier, J., Sakai, N., Robert, F., Kobayashi, T., Gruenberg, J., and Matile, S. (2000) Rapid access to synthetic lysobisphosphatidic acids using P(III) chemistry, *Org. Lett. 2*, 1859−61.
30. Fujisawa, T., Inoue, K., Oka, T., Iwamoto, H., Uraga, T., Kumasaka, T., Inoko, Y., Yagi, N., Yamamoto, M., and Ueki, T. (2000) Small-angle X-ray scattering station at the SPring-8 RIKEN beamline, *J. Appl. Crystallogr. 33*, 797−800.
31. Amemiya, Y., Ito, K., Yagi, N., Asano, K., Wakabayashi, K., Ueji, T., and Endo, T. (1995) Large-aperture TV detector with a beryllium-windowed image intensifier for x-ray diffraction, *Rev. Sci. Instrum. 66*, 2290−2294.
32. Ito, K., Kamikubo, H., Yagi, N., and Amemiya, Y. (2005) Correction method and software for image distortion and non-uniform response in charge-coupled device-based X-ray detectors utilizing X-ray image intensifier, *Jpn. J. Appl. Phys. 44*, 8684−91.
33. Huang, T., Toraya, H., Blanton, T., and Wu, Y. (1993) X-ray powder diffraction analysis of silver behenate, a possible low-angle diffraction standard, *J. Appl. Crystallogr. 26*, 180−4.
34. Imanaka, T., Muto, K., Ohkuma, S., and Takano, T. (1981) Purification and properties of rabbit liver acid-lipase (4-methylumbelliferyl oleate hydrolase), *Biochim. Biophys. Acta 665*, 322−30.
35. Bligh, E. G., and Dyer, W. J. (1959) A rapid method of total lipid extraction and purification, *Can. J. Biochem. Physiol. 37*, 911−7.
36. Ishitsuka, R., Yamaji-Hasegawa, A., Makino, A., Hirabayashi, Y., and Kobayashi, T. (2004) A lipid-specific toxin reveals heterogeneity of sphingomyelin-containing membranes, *Biophys. J. 86*, 296−307.
37. Klein, U., Gimpl, G., and Fahrenholz, F. (1995) Alteration of the myometrial plasma membrane cholesterol content with beta-cyclodextrin modulates the binding affinity of the oxytocin receptor, *Biochemistry 34*, 13784−93.
38. Lipsky, N. G., and Pagano, R. E. (1985) Intracellular translocation of fluorescent sphingolipids in cultured fibroblasts: endogenously synthesized sphingomyelin and glucocerebroside analogues pass through the Golgi apparatus en route to the plasma membrane, *J. Cell Biol. 100*, 27−34.
39. van Meer, G., Stelzer, E. H., Wijnaendts-van-Resandt, R. W., and Simons, K. (1987) Sorting of sphingolipids in epithelial (Madin-Darby canine kidney) cells, *J. Cell Biol. 105*, 1623−35.
40. Kobayashi, T., Pimplikar, S. W., Parton, R. G., Bhakdi, S., and Simons, K. (1992) Sphingolipid transport from the trans-Golgi network to the apical surface in permeabilized MDCK cells, *FEBS Lett. 300*, 227−31.
41. Inokuchi, J., Usuki, S., and Jimbo, M. (1995) Stimulation of glycosphingolipid biosynthesis by L-threo-1-phenyl-2-decanoylamino-1-propanol and its homologs in B16 melanoma cells, *J. Biochem. 117*, 766−73.
42. Rosenwald, A. G., and Pagano, R. E. (1994) Effects of the glucosphingolipid synthesis inhibitor, PDMP, on lysosomes in cultured cells, *J. Lipid Res. 35*, 1232−40.
43. Kok, J. W., Babia, T., Filipeanu, C. M., Nelemans, A., Egea, G., and Hoekstra, D. (1998) PDMP blocks brefeldin A-induced retrograde membrane transport from golgi to ER: evidence for involvement of calcium homeostasis and dissociation from sphingolipid metabolism, *J. Cell Biol. 142*, 25−38.
44. Futerman, A. H., and Pagano, R. E. (1991) Determination of the intracellular sites and topology of glucosylceramide synthesis in rat liver, *Biochem. J. 280*, 295−302.
45. de Wolf, F. A., Maliepaard, M., van Dorsten, F., Berghuis, I., Nicolay, K., and de Kruijff, B. (1990) Comparable interaction of doxorubicin with various acidic phospholipids results in changes of lipid order and dynamics, *Biochim. Biophys. Acta 1096*, 67−80.
46. Takeuchi, R., Imanaka, T., Ohkuma, S., and Takano, T. (1985) Effect of phospholipids on the hydrolysis of cholesterol oleate liquid crystals by lysosomal acid lipase, *J. Biochem. (Tokyo) 98*, 933−8.

47. Greenspan, P., Mayer, E. P., and Fowler, S. D. (1985) Nile red: a selective fluorescent stain for intracellular lipid droplets, *J. Cell Biol. 100*, 965−73.
48. Escola, J. M., Kleijmeer, M. J., Stoorvogel, W., Griffith, J. M., Yoshie, O., and Geuze, H. J. (1998) Selective enrichment of tetraspan proteins on the internal vesicles of multivesicular endosomes and on exosomes secreted by human B-lymphocytes, *J. Biol. Chem. 273*, 20121−7.
49. Kobayashi, T., Vischer, U. M., Rosnoblet, C., Lebrand, C., Lindsay, M., Parton, R. G., Kruithof, E. K., and Gruenberg, J. (2000) The tetraspanin CD63/lamp3 cycles between endocytic and secretory compartments in human endothelial cells, *Mol. Biol. Cell 11*, 1829−43.
50. Lange, Y., and Steck, T. L. (1994) Cholesterol homeostasis. Modulation by amphiphiles, *J. Biol. Chem. 269*, 29371−4.
51. Liscum, L., and Underwood, K. W. (1995) Intracellular cholesterol transport and compartmentation, *J. Biol. Chem. 270*, 15443−6.
52. Underwood, K. W., Andemariam, B., McWilliams, G. L., and Liscum, L. (1996) Quantitative analysis of hydrophobic amine inhibition of intracellular cholesterol transport, *J. Lipid Res. 37*, 1556−68.
53. Goldstein, J. L., Faust, J. R., Dygos, J. H., Chorvat, R. J., and Brown, M. S. (1978) Inhibition of cholesteryl ester formation in human fibroblasts by an analogue of 7-ketocholesterol and by progesterone, *Proc. Natl. Acad. Sci. U.S.A. 75*, 1877−81.
54. Sokol, J., Blanchette-Mackie, J., Kruth, H. S., Dwyer, N. K., Amende, L. M., Butler, J. D., Robinson, E., Patel, S., Brady, R. O., Comly, M. E., et al. (1988) Type C Niemann-Pick disease. Lysosomal accumulation and defective intracellular mobilization of low-density lipoprotein cholesterol, *J. Biol. Chem. 263*, 3411−7.
55. Sato, S. B., Ishii, K., Makino, A., Iwabuchi, K., Yamaji-Hasegawa, A., Senoh, Y., Nagaoka, I., Sakuraba, H., and Kobayashi, T. (2004) Distribution and transport of cholesterol-rich membrane domains monitored by a membrane-impermeant fluorescent polyethylene glycol-derivatized cholesterol, *J. Biol. Chem. 279*, 23790−6.
56. Bhakdi, S., Weller, U., Walev, I., Martin, E., Jonas, D., and Palmer, M. (1993) A guide to the use of pore-forming toxins for controlled permeabilization of cell membranes, *Med. Microbiol. Immunol. 182*, 167−75.
57. Modok, S., Heyward, C., and Callaghan, R. (2004) P-glycoprotein retains function when reconstituted into a sphingolipid- and cholesterol-rich environment, *J. Lipid Res. 45*, 1910−8.
58. Troost, J., Albermann, N., Emil Haefeli, W., and Weiss, J. (2004) Cholesterol modulates P-glycoprotein activity in human peripheral blood mononuclear cells, *Biochem. Biophys. Res. Commun. 316*, 705−11.
59. Assmann, G., and Seedorf, U. (2001) Acid lipase deficiency: Wollman disease and cholesteryl ester storage disease, in *The Metabolic and Molecular Bases of Inherited Disease* (Scriver, C. R., Beasudet, A. L., Sly, W. S., and Valle, D., Eds.) Vol III, McGraw-Hill, New York, Tokyo.
60. Radin, N. S. (2003) Designing anticancer drugs via the achilles heel: ceramide, allylic ketones, and mitochondria, *Bioorg. Med. Chem. 11*, 2123−42.
61. Liour, S. S., and Yu, R. K. (2002) Differential effects of three inhibitors of glycosphingolipid biosynthesis on neuronal differentiation of embryonal carcinoma stem cells, *Neurochem. Res. 27*, 1507−12.
62. Bieberich, E., Freischutz, B., Suzuki, M., and Yu, R. K. (1999) Differential effects of glycolipid biosynthesis inhibitors on ceramide-induced cell death in neuroblastoma cells, *J. Neurochem. 72*, 1040−9.
63. Rani, C. S., Abe, A., Chang, Y., Rosenzweig, N., Saltiel, A. R., Radin, N. S., and Shayman, J. A. (1995) Cell cycle arrest induced by an inhibitor of glucosylceramide synthase. Correlation with cyclin-dependent kinases, *J. Biol. Chem. 270*, 2859−67.
64. Rosenwald, A. G., Machamer, C. E., and Pagano, R. E. (1992) Effects of a sphingolipid synthesis inhibitor on membrane transport through the secretory pathway, *Biochemistry 31*, 3581−90.
65. Dean, M., Hamon, Y., and Chimini, G. (2001) The human ATP-binding cassette (ABC) transporter superfamily, *J. Lipid Res. 42*, 1007−17.
66. Ambudkar, S. V., Kimchi-Sarfaty, C., Sauna, Z. E., and Gottesman, M. M. (2003) P-glycoprotein: from genomics to mechanism, *Oncogene 22*, 7468−85.
67. Urbatsch, I. L., and Senior, A. E. (1995) Effects of lipids on ATPase activity of purified Chinese hamster P-glycoprotein, *Arch. Biochem. Biophys. 316*, 135−40.
68. Rothnie, A., Theron, D., Soceneantu, L., Martin, C., Traikia, M., Berridge, G., Higgins, C. F., Devaux, P. F., and Callaghan, R. (2001) The importance of cholesterol in maintenance of P-glycoprotein activity and its membrane perturbing influence, *Eur. Biophys. J. 30*, 430−42.
69. Gayet, L., Dayan, G., Barakat, S., Labialle, S., Michaud, M., Cogne, S., Mazane, A., Coleman, A. W., Rigal, D., and Baggetto, L. G. (2005) Control of P-glycoprotein activity by membrane cholesterol amounts and their relation to multidrug resistance in human CEM leukemia cells, *Biochemistry 44*, 4499−509.
70. Lange, Y. (1994) Cholesterol movement from plasma membrane to rough endoplasmic reticulum. Inhibition by progesterone, *J. Biol. Chem. 269*, 3411−4.
71. Lavie, Y., Cao, H., Bursten, S. L., Giuliano, A. E., and Cabot, M. C. (1996) Accumulation of glucosylceramides in multidrug-resistant cancer cells, *J. Biol. Chem. 271*, 19530−6.
72. Lucci, A., Cho, W. I., Han, T. Y., Giuliano, A. E., Morton, D. L., and Cabot, M. C. (1998) Glucosylceramide: a marker for multiple-drug resistant cancers, *Anticancer Res. 18*, 475−80.
73. Veldman, R. J., Klappe, K., Hinrichs, J., Hummel, I., van der Schaaf, G., Sietsma, H., and Kok, J. W. (2002) Altered sphingolipid metabolism in multidrug-resistant ovarian cancer cells is due to uncoupling of glycolipid biosynthesis in the Golgi apparatus, *FASEB J. 16*, 1111−3.
74. Liu, Y. Y., Han, T. Y., Giuliano, A. E., and Cabot, M. C. (1999) Expression of glucosylceramide synthase, converting ceramide to glucosylceramide, confers adriamycin resistance in human breast cancer cells, *J. Biol. Chem. 274*, 1140−6.
75. Liu, Y. Y., Han, T. Y., Giuliano, A. E., and Cabot, M. C. (2001) Ceramide glycosylation potentiates cellular multidrug resistance, *FASEB J. 15*, 719−30.
76. Veldman, R. J., Mita, A., Cuvillier, O., Garcia, V., Klappe, K., Medin, J. A., Campbell, J. D., Carpentier, S., Kok, J. W., and Levade, T. (2003) The absence of functional glucosylceramide synthase does not sensitize melanoma cells for anticancer drugs, *FASEB J. 17*, 1144−6.

BI052104Y